Published in final edited form as:
Brain Struct Funct. 2010 March ; 214(2-3): 161–179. doi:10.1007/s00429-010-0245-1.

Changes in dendritic complexity and spine morphology in transgenic mice expressing human wild-type tau

Dara L. Dickstein,
Department of Neuroscience, Mount Sinai School of Medicine, Box 1065, One Gustave L. Levy Place, New York, NY 10029, USA; Computational Neurobiology and Imaging Center, Mount Sinai School of Medicine, New York, NY 10029, USA

Hannah Brautigam,
Department of Neuroscience, Mount Sinai School of Medicine, Box 1065, One Gustave L. Levy Place, New York, NY 10029, USA

Steven D. Stockton Jr.,
Department of Neuroscience, Mount Sinai School of Medicine, Box 1065, One Gustave L. Levy Place, New York, NY 10029, USA

James Schmeidler, and
Department of Psychiatry, Mount Sinai School of Medicine, One Gustave L. Levy Place, New York, NY 10029, USA

Patrick R. Hof
Department of Neuroscience, Mount Sinai School of Medicine, Box 1065, One Gustave L. Levy Place, New York, NY 10029, USA; Computational Neurobiology and Imaging Center, Mount Sinai School of Medicine, New York, NY 10029, USA; Department of Geriatrics and Palliative Care, Mount Sinai School of Medicine, One Gustave L. Levy Place, New York, NY 10029, USA

Abstract

Neurofibrillary tangles (NFTs) are composed of insoluble, hyperphosphorylated aggregates of the microtubule-associated protein tau and are present in various neurodegenerative diseases, including Alzheimer's disease (AD). To investigate how tau affects neuronal function during NFT formation and subsequent neurodegeneration, we examined the morphology, spine density, spine type, and spine volume of layer III pyramidal neurons from the prefrontal cortex of mice expressing wild-type human tau (htau) over time. There were no significant alterations in apical dendritic arbor length in 3-, 6-, and 12-month-old htau mice; however, 12-month-old mice exhibited more complex arborization patterns. In addition, we observed a shift in spine morphology with fewer mushroom and more thin spines in both apical and basal dendrites as a function of htau accumulation. Interestingly, there was an overall decrease in volume of spines from 3 to 12 months. However, the volume of mushroom spines decreased from 3 to 6 months and increased from 6 to 12 months. This increase in complexity and branching in 12-month-old mice and the increase of volume of mushroom spines may represent compensatory mechanisms in the remaining intact neurons. As such, the accumulation of phosphorylated tau over time may contribute to the cognitive decline observed in AD by affecting neuronal structure and synaptic properties. Such alterations in dendrites and spines may result in the deterioration of neuronal function observed in AD, and provide a morphologic substrate for the relationship between synaptic integrity and cognitive decline.

dara.dickstein@mssm.edu .

Keywords

Alzheimer's disease; Neurofibrillary tangles; Tau; Transgenic mice; Dendrites; Spines

Introduction

The abnormal aggregation and accumulation of the microtubule-associated protein tau into neurofibrillary tangles (NFTs) is a defining pathological feature of many neurodegenerative diseases such as Alzheimer's disease (AD), frontotemporal dementia with parkinsonism linked to chromosome 17 (FTDP-17), Pick's disease, and progressive supranuclear palsy. The tau protein is localized to neuronal axons as well as to the somatodendritic compartment, and plays a key role in microtubule assembly and stabilization, cellular trafficking, maintenance of neuronal morphology, and the formation of axonal and dendritic processes (reviewed in Gendron and Petrucelli 2009). Numerous mutations in the tau gene have been discovered and are linked to FTDP-17; however, no known mutations in the tau gene have been associated with AD. In AD, NFTs are distributed primarily to the hippocampus, entorhinal cortex, and association regions of the neocortex. It has been proposed that in AD, abnormalities in tau induce the formation of paired helical filaments (PHFs) and the subsequent formation of NFTs leading to neuronal loss and dementia (Goedert and Spillantini 2000; Spillantini et al. 2000). Interestingly, it has been shown that the distribution and number of NFT inclusions correlate better with neuronal loss, synapse loss, and the degree of cognitive impairment observed in AD than do amyloid deposits (Buée et al. 2000; Bussière et al. 2002; Lee et al. 2001). While evidence shows that the hyperphosphorylation and aggregation of tau into NFT is neurotoxic, the exact neurotoxic species of tau and exact mechanisms by which this species of tau causes neurodegeneration remains elusive (Buée et al. 2000). Many tau transgenic mouse models have been created to address these underlying questions. For example, mice harboring the FTDP-17 P301L mutation have been generated and present with behavioral deficits, NFT-like inclusions, and neuronal death (Götz et al. 2000, 2001, 2004; Spires et al. 2006; Yoshiyama et al. 2005). Other mice which expressed non-mutated human tau have also been generated. One such model, created by Andorfer et al. (2003, 2005), expresses all six isoforms of non-mutant human tau (htau) and no mouse tau. These mice undergo an age-related accumulation of phosphorylated tau and PHFs in the somatadendritic regions of neurons and present with the same regional distribution of tau pathology as seen in human AD cases (Andorfer et al. 2003, 2005). In addition, these animals exhibit a decrease in cortical thickness, a decrease in the thickness of the corpus callosum, an increase in ventricle size, and a significant reduction in neuronal numbers with age (Andorfer et al. 2005). Age-dependent cognitive and physiological impairments have also been reported as indicated by impaired performance in the Morris water maze and object recognition and perturbed basal synaptic transmission and induction of long-term potentiation (LTP) (Polydoro et al. 2009).

It has been suggested that loss of dendritic spines or structural reorganization of spines and disturbances in synaptic signaling are important for learning and memory and may be one of the first signs of AD (Nimchinsky et al. 2002; Segal 2005; Yuste and Bonhoeffer 2001). In fact, many studies have demonstrated that synaptic or spine loss is a better indicator of cognitive impairment than amyloid pathology (Akram et al. 2008; Scheff and Price 2006; Scheff et al. 2007; Terry et al. 1991), thereby suggesting that changes in spine morphology and distribution may be critical in understanding the synaptic toxicity observed in AD. To address the potential connection between the accumulation of hyperphosphorylated tau on the architecture of neuronal dendrites and on spine density and morphology, we examined htau mice at various ages, beginning at 3 months when hyperphosphorylated tau has been shown to begin to accumulate (Andorfer et al. 2003). We found that with age the

accumulation of tau in neuron somata has an effect on dendrite morphology and on spine density in pyramidal cells of the prefrontal cortex (PFC). In addition, we show a shift in spine type from stable mushroom spines to thin spines indicating a change in the ability to sustain strong synaptic activity.

Materials and methods

Animals

This study used 3-, 6-, and 12-month-old htau mice and littermate controls (Jackson Laboratories, Bar Harbor, ME, USA; see Table 1 for sample size for each analysis). The htau mouse was generated by crossing two existing and established mouse lines, line 8c (Duff et al. 2000), which contains the entire human tau transgene under control of the tau promoter, and the tau knockout mouse, which has a targeted disruption of exon 1 of mouse tau (Tucker et al. 2001) using cDNA for the enhanced green fluorescent protein (EGFP). The resulting mouse expresses all six isoforms of non-mutated human tau and no mouse tau (Andorfer et al. 2003). Mice were fed lab chow ad libitum and kept under a 12 h light/dark cycle. All animal procedures were conducted in accordance with the National Institute of Health Guidelines for the Care and Use of Experimental Animals approved by the Institutional Animal Care and Use Committee at Mount Sinai School of Medicine.

Animals were anesthetized with a euthanizing dose of choral hydrate (0.1 ml of a 15% solution, i.p.), and perfused transcardially at a rate of 5 ml/min with ice cold 1% paraformaldehyde in 0.1 M phosphate-buffered saline (PBS, pH 7.4) for 1 min followed by 4% paraformaldehyde in 0.1 M PBS for 12 min. The brains were carefully removed from the skull and hemisected. The left hemisphere was postfixed for 6 h at 4°C in 4% paraformaldehyde in PBS with 0.125% glutaraldehyde, stored in PBS overnight and sectioned at 200 μm on a Vibratome (Leica VT1000S, Bannockburn, IL, USA) for cell loading experiments. For consistency within the study, the right hemisphere was used for all immunohistochemical analyses while the left hemisphere was used for all cell loading experiments. The right hemisphere was postfixed overnight at 4°C in 4% paraformaldehyde, and used for immunohistochemical analysis.

Immunocytochemistry

The right hemisphere of each animal was sectioned coronally at 50 μm on a Vibratome (Leica), with every fourth section being stained for Nissl substance with 0.2% cresyl violet. Additional sections containing the PFC were immunostained using the monoclonal mouse IgG antibody AT8, raised against PHF-tau phosphorylated at Ser202 and Thr205 (Pierce Biotechnology, Rockford, IL, USA). Briefly, free-floating sections were incubated for 1 h in a blocking solution of 20% normal goat serum (Sigma-Aldrich, St. Louis, MO, USA), 1.8% mouse Ig blocking reagent with 8% protein concentrate (Vector M.O.M. Kit, Vector Laboratories, Burlingame, CA, USA), and 0.3% Triton-X 100 in 0.1 M phosphate-buffered saline (PBS). After blocking, sections were incubated in AT8 (1:250) overnight at room temperature. Sections were next rinsed in 0.1 M PBS, and then incubated in a biotinylated goat-anti-mouse secondary antibody for 30 min (1:200; Dako, Glostrup, Denmark). All sections were processed using the avidin–biotin peroxidase method (ABC Kit, Vector Laboratories), after which immunoreactivity was visualized using via the nickel-stabilized 3,3′-diaminobenzidine reaction product.

A 1:4 systematic-random section series was mounted for each animal on 2% gelatin-subbed slides and permitted to dry overnight at room temperature. The slides were dehydrated through a series of increasingly concentrated ethanol solutions followed by incubation in chloroform to remove endogenous lipids. Sections were then rehydrated through a series of

increasingly dilute ethanol solutions and stained for Nissl substance using a 0.2% cresyl violet acetate solution (Sigma-Aldrich) for 6 min. After a quick (≤2 min) wash in dH_2O, sections were again dehydrated, rinsed in a 95% ethanol solution with 17.4 N acetic acid until differentiated, further dehydrated through D-limonene, and coverslipped with DePeX mounting medium (Fluka, Milwaukee, WI, USA).

Intracellular dye injections

After fixation brain sections were serially cut at a thickness of 200 μm on a Vibratome (Leica) and stored at 4°C in PBS until ready for use. For intracellular injections, sections were incubated in 4′,6-diamidino-2-phenylindole (DAPI; Sigma, St. Louis, MO, USA) for 5 min to reveal the cytoarchitectural features of layer III of the PFC. The sections were then mounted on nitrocellulose paper and immersed in ice-cold 0.1 M PBS. Pyramidal neurons in layer III of the PFC were injected with an intracellular iontophoretic injection of 5% Lucifer Yellow (Molecular Probes, Eugene, OR, USA) in distilled water under a DC current of 3–8 nA for 5–10 min, or until dye had completely filled distal processes and no further loading was observed (Duan et al. [2002],2003;Hao et al. 2006; Radley et al. 2004,2006). 5–10 neurons were injected per slice and placed far enough apart to avoid overlapping of their dendritic trees. Brain sections containing loaded neurons were then mounted on gelatin-coated glass slides and cover slipped in PermaFluor mounting medium (Immunotech, Marseille, France).

Neuronal and dendritic reconstruction

In order for a loaded neuron to be included in the analysis, it had to satisfy the following criteria: (1) lie within layer III of the PFC as defined by cytoarchitectural characteristics; (2) demonstrate complete filling of dendritic tree, as evidenced by well-defined endings; (3) demonstrate intact primary and secondary branches; (4) demonstrate intact tertiary branches, with the exception of branches that extended beyond 50 μm in radial distance from the cell soma (Duan et al. [2002],2003;Hao et al. 2006; Radley et al. 2004,2006). Neurons meeting these criteria were reconstructed in three-dimension (3D) with a 63X/1.4 N.A., Plan-Apochromat oil immersion objective on a Zeiss Axiophot 2 microscope equipped with a motorized stage, video camera system, and Neurolucida morphometry software (MBF Bioscience, Williston, VT, USA). Using NeuroExplorer software (MBF Bioscience) total dendritic length, number of intersections, and the amount of dendritic material per radial distance from the soma in 30-μm increments (Sholl 1953) were analyzed in order to assess morphological cellular diversity and potential differences among animal groups.

Confocal microscopy and spine acquisition

Using an approach that precludes sampling bias of spines, dendritic segments were selected with a systematic-random design (Duan et al. 2003; Hao et al. 2006; Radley et al. 2006). Dendritic segments, 20–25 μm in length, were imaged on a Zeiss LSM 410 confocal microscope (Zeiss, Thornwood, NY, USA) using a 100X/1.4 N.A. Plan-Apochromat objective with a digital zoom of 5 and an Ar/Kr laser at an excitation wavelength of 488 nm. All confocal stacks were acquired at 512 × 512 pixel resolution with a *z*-step of 0.1 μm, a pinhole setting of one Airy unit and optimal settings for gain and offset. All confocal stacks included approximately 1 μm above and below the identified dendritic segment. On average four *z*-stacks were imaged per neuron. In order for a dendritic segment to be optically imaged, it had to satisfy the following criteria: (1) the entire segment had to fall within a depth of 50 μm; (2) dendritic segments had to be either parallel or at acute angles to the coronal surface of the section; and (3) segments did not overlap other segments that would obscure visualization of spines (Radley et al. 2006, 2008). Confocal stacks were then deconvolved using an iterative blind deconvolution algorithm (AutoDeblur version 8.0.2; MediaCybernetics, Bethesda, MD, USA). This step is necessary since in the raw image, the image spread in the *Z* plane would limit the precise interpretation of 3D spine morphology.

The deconvolution step converts out of focus signal to focused signal and results in images where dendritic diameters and spine shapes are well defined and can be accurately analyzed (Rodriguez et al. 2003, 2006, 2008).

Spine analysis

After deconvolution, confocal stacks were analyzed with NeuronStudio (Rodriguez et al. [2006],2008;Wearne et al. 2005; http://www.mssm.edu/cnic) to examine global and local morphometric characteristics of dendrites and spines such as dendritic spine densities, dendritic spine shape (stubby, mushroom, and thin), and dendritic spine volume. This software allows for automated digitization and reconstructions of 3D neuronal morphology from multiple confocal stacks on a spatial scale and averts the subjective errors encountered during manual tracing using a Rayburst-based spine analysis (Rodriguez et al. 2003,2006,2008). At least three dendritic segments per apical and per basal dendrite were analyzed per cell with each segment manually inspected and appropriate corrections made using the NeuronStudio interface.

Statistical analysis

Scores for analyses for each htau transgenic (htau) animal and their wild type (wt) counterparts were obtained by taking the average of the data from all neurons for each animal. An independent samples *t* test was performed on spine density, spine percentage, spine volume, and dendritic length. For each age, separately, Sholl analysis data were compared by repeated measures ANOVA with genotype (htau vs. wt) as the between-group factor and distance from the soma as the repeated-measures factor. In comparing the htau mice at all three ages, Sholl analysis data were compared by repeated measures ANOVA with age (3 vs. 6 vs. 12 months) as the independent variable, genotype as the between group factor, and distance from the soma as the repeated-measures factor. The α level was set at 0.05 for all analyses in the study, and all data were represented as mean ± SEM. Tables 2 and 3 summarize the statistically significant results of this dataset.

Results

Phosphorylated tau in htau mice

Cresyl violet staining of adjacent sections showed no apparent changes in neuronal densities in htau mice compared to wt. In addition, there were also no apparent changes in neuronal densities over time (Fig. 1a, b). Further quantitative stereologic analysis is currently being undertaken; however, preliminary data show no significant neuronal loss (data not shown). It has been demonstrated previously that htau mice develop pretangles and early NFT pathology in an age-dependent manner in the hippocampus and neocortex as early as 6 weeks of age (Andorfer et al. 2003, 2005). Our findings are consistent with these earlier studies in the htau mouse. We confirmed by immunohistochemistry that all htau animals from the three age groups exhibited tau pathology, in particular, the somatodendritic accumulation of AT8-immunoreactive phosphorylated tau in the PFC and hippocampus of htau mice compared to controls. These AT8-positive aggregates were seen in all age groups and did accumulate over time (Fig. 1c, d). At 3 months of age, the AT8 labeling was seen in the somata and apical dendrites of pyramidal cells of the hippocampus and neocortex. The pattern of AT8 immunoreactivity changed with age with a more pronounced accumulation in the dendrites, resembling that which occurs in early stages of NFT formation in the human brain.

Tau-associated dendritic pathology in the htau cortex

Examples of PFC dendritic arbor reconstructions and apical dendrite dendrograms are depicted in Fig. 2. All neurons were clearly identifiable as layer III pyramidal cells and lied within the same region of the PFC. Detailed analyses of the various morphometric parameters (i.e., length and complexity) of individual apical and basal dendrites at 3 months of age showed no significant differences between htau mice and wt mice (Figs. 2a, b, 3). At 6 months, there was a statistically significant difference in basal dendritic length between htau and wt mice [$t_{(9)} = -2.952$, $p = 0.016$], with htau mice having shorter basal dendritic length compared to wt littermates. However, there was no difference in apical dendritic length between the groups (Figs. 2c, d, 4a, b). Further analyses revealed no significant difference between genotypes or interaction of genotype with distance from the soma for apical or basal dendritic Sholl analyses, or for apical or basal intersections (Fig. 4c–f). Interestingly, at 12 months of age, where there is an abundant amount of hyperphosphorylated tau as indicated by AT8 staining, there was no significant difference in apical or basal dendritic length between htau and wt mice (Figs. 2e, f, 5a, b). However, a repeated-measures ANOVA found a statistically significant interaction of genotype with distance from the soma [$F_{(4.68,42.10)} = 3.86$, $p = 0.007$; Fig. 5c, e] in the apical dendrites of htau mice compared to wt with the htau mice having longer dendritic length and more branching complexity from 30 to 120 μm, and shorter dendritic length with sparse branching at the apical tuft. No significant difference was observed in basal dendrites (Fig. 5d, f).

When comparing means from 3-, 6-, and 12-month-old htau mice, there were no significant differences in apical and basal dendritic length over time (Table 3; Figs. 2a, c, e, 6a, b). Further, Sholl analysis of apical dendrites for htau with age as the independent variable showed an effect of age with distance from the soma with 12-month-old mice having the longest dendritic length from 30 to 150 μm and the shortest dendritic length from 180 to 210 μm compared to the 3- and 6-month-old mice [repeated-measures ANOVA, $F_{(6.29,40.49)} = 2.15$, $p = 0.066$; Fig. 6c]. This trend was also observed in the degree of complexity of the apical tree and reached significance at 60–90 μm from the soma [$F_{(7.40,48.10)} = 2.36$, $p = 0.035$; Fig. 6d]. No significant difference by age or interaction of age with distance from the soma was observed in basal dendrites in both dendritic length and dendritic complexity (Fig. 6d, f). In contrast to other studies which showed significant dendritic atrophy in mutant tau mice, there was no overt significant effect by age and accumulation of phosphorylated tau on dendritic morphology in htau animals.

Spine density, spine volume, and percent of spine type

The assessment of dendritic spine number per unit length, spine type, and spine volume was performed on 3D reconstructed images (as shown in Fig. 7) from apical and basal dendrites from htau and wt mice at 3, 6, and 12 months of age using NeuronStudio (Table 2). Statistical analysis indicated no statistically significant differences in apical or basal total spine density in 3-, 6-, and 12-month-old htau mice compared to controls (Figs. 8a, b, 9a, b, 10a, b).

Dendritic spines can be subdivided into different categories depending on their shape: stubby, thin, and mushroom (Peters and Kaiserman-Abramof 1970). It is thought that LTP, which is associated with learning and memory storage, takes place in spines and that different spine types facilitate different levels of plasticity (Peters and Kaiserman-Abramof 1970). Thus, changes in the type of spines can have adverse effects to learning and memory, and may account for the behavioral deficits that occur in these animals (Polydoro et al. 2009). We evaluated the types of spines, shifts in spine types, as well as the volumes of spines at all time points in htau mice and wt (Table 2). At 3 months of age, there were no significant changes in the amount of thin or mushroom spines on both the apical and basal

dendrites between htau and wt mice. There was also no difference in apical stubby, thin, or mushroom spine volume, or basal thin or mushroom spine volume (Fig. 8). However, we did see a definite trend in the percent of apical and basal stubby spines, with htau mice having a higher percent than wt mice, and in basal stubby volume with htau once again having a larger volume compared to wt mice. At 6 months, there were no statistically significant changes in the spine densities, spine types, and spine volumes for both apical and basal dendrites between htau and wt mice (Fig. 9a–d). At 12 months, there was no difference in the number of basal stubby or mushroom spines or in the number of apical thin or mushroom spines (Fig. 10c, d). We did find a decrease in the number of basal thin spines in htau mice compared to wt mice [$t_{(6)} = -2.824$, $p = 0.03$; Fig. 10d]. The htau mice showed a larger percent of apical stubby spine compared to wt, which was very near significance [$t_{(6)} = 2.416$, $p = 0.052$; Fig. 10c]. As for spine volume, there was no significant difference in basal stubby, thin, or mushroom types; there was also no significant difference in apical thin or mushroom spines; however, for stubby spines, htau mice showed a larger spine volume compared to wt mice approaching significance (Fig. 10e, f).

When comparing means from 3-, 6-, and 12-month-old htau mice (Table 3), there was a significant increase in apical spine density with no changes in basal density [$F_{(2,10)} = 10.751$, $p = 0.003$; Figs. 7, 11a, b]. A Bonferroni post-hoc test revealed that the 3-month-old mice ($M = 1.40$) had a statistically significant smaller apical total spine density compared to 12-month-old htau mice ($M = 1.96$, $p = 0.003$). Analysis of spine types revealed an overall increase in the number of thin spines and a decrease in the number of mushroom spines with the accumulation of tau pathology (Fig. 11c, d) in both apical and basal dendrites. There was no significant difference in apical spine volumes with age. In contrast, all basal spine types exhibited statistically significant changes [stubby volume: $F_{(2,10)} = 12.240$, $p = 0.002$; thin volume: $F_{(2,10)} = 5.574$, $p = 0.024$; mushroom volume: $F_{(2,10)} = 6.971$, $p = 0.013$]. Interestingly, for both apical and basal dendrites, there was a trend observed that 6- and 12-month-old mice have a larger thin volume than 3-month-old mice. This larger volume may represent the shrinking of the mushroom spine to a thin spine, and may explain the shift from mushroom to thin spines with no overt loss in density. In addition, 12-month-old mice have significantly larger mushroom spines then younger animals. This increase in volume may be a way for the remaining competent neurons to compensate for neurons that have severe tau pathology.

Discussion

There is compelling evidence that the aberrant hyperphosphorylation and aggregation of the tau protein in AD and other tauopathies leads to neurodegeneration (Buée et al. 2000; Gendron and Petrucelli 2009; Goedert and Spillantini 2000). Many studies have shown that tau pathology and the number of NFTs correlates with cognitive decline and reflect cognitive deficits better than the accumulation Aβ into plaques (Akram et al. 2008; Arriagada et al. 1992; Bancher et al. 1993; Braak and Braak 1991; Bussiere et al. 2002). However, the influence of tau pathology on neuronal connectivity remains elusive. Recently, Polydoro et al. (2009) suggested that developing tau pathology may cause cognitive impairment by means of disruption of synaptic transmission. The purpose of this study was to determine the affect of aggregating PHFs and NFTs on synapses and neurons. To this end, we analyzed dendrite and spine morphology in the htau mouse model at different stages of tau pathology. We found no significant differences in apical or basal dendritic length over time; however, 12-month-old mice did have more complex branching patterns at proximal distances from the soma in apical dendrites. This is the first demonstration of what structural changes occur during aberrant hyperphosphorylation and aggregation of wt tau over time. Other studies in mice overexpressing the P301L mutation (rTg4510) have investigated morphological changes and show conflicting results. Rocher et al. (2010) examined the

same region as we did and found significant atrophy of apical dendritic tufts in layer I, as well as reduced dendritic complexity and length. These changes were present in both neurons that exhibited NFTs and in neurons that did not (Rocher et al. 2010). In an earlier study in the CA1 and dentate gyrus, there was a slight increase in terminal apical dendritic length with no overall difference in total dendritic length or number of dendrites (Boekhoorn et al. 2006). The main difference between these studies and the present one is the choice of transgenic mouse model. The htau mouse model used in our study harbors no mutations in the human tau it expresses, a state similar to what is observed in AD and normal aging. Moreover, this animal expresses all six isoforms of tau, a scenario that closely mimics what occurs in humans. As in humans, these mice accumulate hyperphosphorylated tau over time and develop NFTs in regions of the brain that are affected in the human disease (Andorfer et al. 2003, 2005). Although mutations in the tau gene occur in many tauopathies such as FTDP-17, Pick's disease, and progressive supranuclear palsy, no mutations have been observed in AD (Shahani and Brandt 2002). As each of these tauopathies exhibits different regional patterns of NFTs formation and cellular degeneration (Gendron and Petrucelli 2009) and since there are functional differences between normal and mutated tau (Dayanandan et al. 1999; Hong et al. 1998), it is plausible that the exact mechanism by which tau interacts with other proteins and exerts its toxicity may be somewhat different, although based on the aggregation and accumulation of NFTs. Recently, Tackenberg and Brandt (2009) have demonstrated that in conjunction with Aβ, the toxicity of wt and different mutants of the tau protein (P301L and R406W) is mediated by divergent pathways downstreamof *N*-methyl-D-aspartate (NMDA) receptor activation. In addition, while the tau mouse models that have mutations in the tau gene do exhibit behavioral deficits and morphological changes, they also exhibit motor impairments (Ramsden et al. 2005), conditions which do not parallel with what is observed in human AD. Other differences in finding between these studies can be explained further by the age of the experimental animals, the methodology employed (e.g., estimates derived from Golgi impregnations versus intracellular injections and confocal microscopy), or the subpopulation of cells examined. While there is considerable diversity of pyramidal cells in the PFC and differences in their dendritic length and spine densities (Soloway et al. 2002), the differences among neurons located in the deeper third of layer III is likely to be considerably smaller. These neurons constitute for the most large output corticocortical neurons, as shown in Duan et al. (2002, 2003) and Kabaso et al. (2009), and as a group they are comparable. Of note, the neurons analyzed in this study were taken very consistently from the deep third of layer III in the mouse PFC, and as such represent a similarly consistent sample of cells with rather comparable morphology and size.

Studies examining the changes in spine density as a result of tau toxicity are conflicting. In vitro studies have demonstrated that the overexpression of htau results in a loss of spines (Eckermann et al. 2007) while ex vivo studies only demonstrate tau-mediated changes in spine density in the presence of Aβ and not when expressed alone (Tackenberg and Brandt 2009). Studies in transgenic mice expressing mutated tau have also shown changes in spine density (Eckermann et al. 2007; Thies and Mandelkow 2007). In contrast, Rocher et al. (2010) have recently reported that changes in spine density in the rTg4510 mouse were independent of the presence of NFTs. Once again, these studies involved the overexpression of mutated forms of human tau, whereas we are using a mouse expressing non-mutated tau. Although we show no difference in spine density between htau and wt mice, we do show that in the htau mice there is a shift from mushroom spines with the aggregation of abnormal tau, which is in agreement with the study of (Tackenberg and Brandt 2009). We also show a slight decrease in the volume of spines with aggregation of phosphorylated tau. This shift in spine morphology and spine volume can explain the cognitive deficits and impairment in LTP reported in this mouse model (Polydoro et al. 2009). Mushroom spines represent more stable "memory" spines as they have a larger postsynaptic density (PSD) than thin spines

and contain more α-amino-3-hydroxy-5-methyl-4-isoxazolepropionic acid (AMPA) receptors that are important in conferring postsynaptic cell excitability, the expression of synaptic plasticity and synaptic strength (Genoux and Montgomery 2007; Sommer et al. 1992; Tackenberg et al. 2009). Interestingly, when examined by spine type, our data show that at later stages of pathology there is an increase in the volume of mushroom and thin spines. This increase in spine volume may be the way these neurons compensate for the loss of synapses occurring along their dendrites. This presence of large spines is also seen in human AD cases, where many spines appear to be distorted, dystrophic, and larger than normal in size (Baloyannis et al. 2007). Furthermore, the larger volume of thin spines observed in the htau mouse during increasing tau pathology could be the regression of mushroom spines into thin spines. Future studies using immunoelectron microscopy are needed in order to assess these morphological changes and changes in receptor expression, the presence of a functional synapse, the strength of the synapse, and determine the possible mechanism by which these changes are occurring.

In summary, we have identified alterations in dendritic architecture and shifts in spine morphology as tau accumulates into aggregates. These data provide evidence that the abnormal accumulation of hyperphosphorylated tau and NFTs are likely to have an adverse effect on the synaptic capabilities of the cell and may contribute to the cognitive decline and neurodegeneration observed in AD and other tauopathies. While the changes we observed as a result of wt tau expression are slight, it is important to recognize that in conjunction with other pathologies that occur in AD, such as Aβ toxicity and aggregation and inflammation, these effects can be greatly exacerbated. Defining the physiological repercussions involved in tau accumulation and pathology and the mechanism by which these changes occur is vital to our understanding of tau-mediated neurodegeneration in AD.

Acknowledgments

We thank W.G.M Janssen for expert technical assistance, A. Rodriguez and D. Ehlenberger for help with Neuron-Studio, and the late Dr. S.L. Wearne for developing the algorithms used in our analyses and her invaluable input to these studies. This work was supported by NIH grants AG02219, AG05138, MH58911, and MH071818.

Abbreviations

AD	Alzheimer's disease
Aβ	Amyloid beta protein
NFTs	Neurofibrillary tangles
FTDP-17	Frontotemporal dementia with parkinsonism linked to chromosome 17
PHFs	Paired helical filaments
EGFP	Enhanced green fluorescent protein
PBS	Phosphate-buffered saline
PFC	Prefrontal cortex
3D	Three-dimensional
wt	Wild-type

References

Akram A, Christoffel D, Rocher AB, Bouras C, Kövari E, Perl DP, Morrison JH, Herrmann FR, Haroutunian V, Giannakopoulos P, Hof PR. Stereologic estimates of total spinophilin-

immunoreactive spine number in area 9 and the CA1 field: relationship with the progression of Alzheimer's disease. Neurobiol Aging 2008;29(9):1296–1307. [PubMed: 17420070]

Andorfer C, Kress Y, Espinoza M, de Silva R, Tucker KL, Barde YA, Duff K, Davies P. Hyperphosphorylation and aggregation of tau in mice expressing normal human tau isoforms. J Neurochem 2003;86(3):582–590. [PubMed: 12859672]

Andorfer C, Acker CM, Kress Y, Hof PR, Duff K, Davies P. Cell-cycle reentry and cell death in transgenic mice expressing nonmutant human tau isoforms. J Neurosci 2005;25(22):5446–5454. [PubMed: 15930395]

Arriagada PV, Growdon JH, Hedley-Whyte ET, Hyman BT. Neurofibrillary tangles but not senile plaques parallel duration and severity of Alzheimer's disease. Neurology 1992;42(3 Pt 1):631–639. [PubMed: 1549228]

Baloyannis SJ, Costa V, Mauroudis I, Psaroulis D, Manolides SL, Manolides LS. Dendritic and spinal pathology in the acoustic cortex in Alzheimer's disease: morphological and morphometric estimation by Golgi technique and electron microscopy. Acta Otolaryngol 2007;127(4):351–354. [PubMed: 17453452]

Bancher C, Braak H, Fischer P, Jellinger KA. Neuropathological staging of Alzheimer lesions and intellectual status in Alzheimer's and Parkinson's disease patients. Neurosci Lett 1993;162(1–2): 179–182. [PubMed: 8121624]

Boekhoorn K, Terwel D, Biemans B, Borghgraef P, Wiegert O, Ramakers GJ, de Vos K, Krugers H, Tomiyama T, Mori H, Joels M, van Leuven F, Lucassen PJ. Improved long-term potentiation and memory in young tau-P301L transgenic mice before onset of hyperphosphorylation and tauopathy. J Neurosci 2006;26(13):3514–3523. [PubMed: 16571759]

Braak H, Braak E. Demonstration of amyloid deposits and neurofibrillary changes in whole brain sections. Brain Pathol 1991;1(3):213–216. [PubMed: 1669710]

Buée L, Bussière T, Buée-Scherrer V, Delacourte A, Hof PR. Tau protein isoforms, phosphorylation and role in neurodegenerative disorders. Brain Res Brain Res Rev 2000;33(1):95–130. [PubMed: 10967355]

Bussière T, Friend PD, Sadeghi N, Wicinski B, Lin GI, Bouras C, Giannakopoulos P, Robakis NK, Morrison JH, Perl DP, Hof PR. Stereologic assessment of the total cortical volume occupied by amyloid deposits and its relationship with cognitive status in aging and Alzheimer's disease. Neuroscience 2002;112(1):75–91. [PubMed: 12044473]

Dayanandan R, Van Slegtenhorst M, Mack TG, Ko L, Yen SH, Leroy K, Brion JP, Anderton BH, Hutton M, Lovestone S. Mutations in tau reduce its microtubule binding properties in intact cells and affect its phosphorylation. FEBS Lett 1999;446(2–3):228–232. [PubMed: 10100846]

Duan H, Wearne SL, Morrison JH, Hof PR. Quantitative analysis of the dendritic morphology of corticocortical projection neurons in the macaque monkey association cortex. Neuroscience 2002;114(2):349–359. [PubMed: 12204204]

Duan H, Wearne SL, Rocher AB, Macedo A, Morrison JH, Hof PR. Age-related dendritic and spine changes in corticocortically projecting neurons in macaque monkeys. Cereb Cortex 2003;13(9): 950–961. [PubMed: 12902394]

Duff K, Knight H, Refolo LM, Sanders S, Yu X, Picciano M, Malester B, Hutton M, Adamson J, Goedert M, Burki K, Davies P. Characterization of pathology in transgenic mice overexpressing human genomic and cDNA tau transgenes. Neurobiol Dis 2000;7(2):87–98. [PubMed: 10783293]

Eckermann K, Mocanu MM, Khlistunova I, Biernat J, Nissen A, Hofmann A, Schonig K, Bujard H, Haemisch A, Mandelkow E, Zhou L, Rune G, Mandelkow EM. The beta-propensity of Tau determines aggregation and synaptic loss in inducible mouse models of tauopathy. J Biol Chem 2007;282(43):31755–31765. [PubMed: 17716969]

Gendron TF, Petrucelli L. The role of tau in neurodegeneration. Mol Neurodegener 2009;4:13. [PubMed: 19284597]

Genoux D, Montgomery JM. Glutamate receptor plasticity at excitatory synapses in the brain. Clin Exp Pharmacol Physiol 2007;34(10):1058–1063. [PubMed: 17714094]

Goedert M, Spillantini MG. Tau mutations in frontotemporal dementia FTDP-17 and their relevance for Alzheimer's disease. Biochim Biophys Acta 2000;1502(1):110–121. [PubMed: 10899436]

Götz J, Barmettler R, Ferrari A, Goedert M, Probst A, Nitsch RM. In vivo analysis of wild-type and FTDP-17 tau transgenic mice. Ann N Y Acad Sci 2000;920:126–133. [PubMed: 11193141]

Götz J, Chen F, van Dorpe J, Nitsch RM. Formation of neurofibrillary tangles in P301 l tau transgenic mice induced by Abeta 42 fibrils. Science 2001;293(5534):1491–1495. [PubMed: 11520988]

Götz J, Streffer JR, David D, Schild A, Hoerndli F, Pennanen L, Kurosinski P, Chen F. Transgenic animal models of Alzheimer's disease and related disorders: histopathology, behavior and therapy. Mol Psychiatry 2004;9(7):664–683. [PubMed: 15052274]

Hao J, Rapp PR, Leffler AE, Leffler SR, Janssen WG, Lou W, McKay H, Roberts JA, Wearne SL, Hof PR, Morrison JH. Estrogen alters spine number and morphology in prefrontal cortex of aged female rhesus monkeys. J Neurosci 2006;26(9):2571–2578. [PubMed: 16510735]

Hong M, Zhukareva V, Vogelsberg-Ragaglia V, Wszolek Z, Reed L, Miller BI, Geschwind DH, Bird TD, McKeel D, Goate A, Morris JC, Wilhelmsen KC, Schellenberg GD, Trojanowski JQ, Lee VM. Mutation-specific functional impairments in distinct tau isoforms of hereditary FTDP-17. Science 1998;282(5395):1914–1917. [PubMed: 9836646]

Kabaso D, Coskren PJ, Henry BI, Hof PR, Wearne SL. The electrotonic structure of pyramidal neurons contributing to prefrontal cortical circuits in macaque monkeys is significantly altered in aging. Cereb Cortex 2009;19(10):2248–2268. [PubMed: 19150923]

Lee VM, Goedert M, Trojanowski JQ. Neurodegenerative tauopathies. Annu Rev Neurosci 2001;24:1121–1159. [PubMed: 11520930]

Nimchinsky EA, Sabatini BL, Svoboda K. Structure and function of dendritic spines. Annu Rev Physiol 2002;64:313–353. [PubMed: 11826272]

Peters A, Kaiserman-Abramof IR. The small pyramidal neuron of the rat cerebral cortex. The perikaryon, dendrites and spines. Am J Anat 1970;127(4):321–355. [PubMed: 4985058]

Polydoro M, Acker CM, Duff K, Castillo PE, Davies P. Age-dependent impairment of cognitive and synaptic function in the htau mouse model of tau pathology. J Neurosci 2009;29(34):10741–10749. [PubMed: 19710325]

Radley JJ, Sisti HM, Hao J, Rocher AB, McCall T, Hof PR, McEwen BS, Morrison JH. Chronic behavioral stress induces apical dendritic reorganization in pyramidal neurons of the medial prefrontal cortex. Neuroscience 2004;125(1):1–6. [PubMed: 15051139]

Radley JJ, Rocher AB, Miller M, Janssen WG, Liston C, Hof PR, McEwen BS, Morrison JH. Repeated stress induces dendritic spine loss in the rat medial prefrontal cortex. Cereb Cortex 2006;16(3):313–320. [PubMed: 15901656]

Radley JJ, Rocher AB, Rodriguez A, Ehlenberger DB, Dammann M, McEwen BS, Morrison JH, Wearne SL, Hof PR. Repeated stress alters dendritic spine morphology in the rat medial prefrontal cortex. J Comp Neurol 2008;507(1):1141–1150. [PubMed: 18157834]

Ramsden M, Kotilinek L, Forster C, Paulson J, McGowan E, SantaCruz K, Guimaraes A, Yue M, Lewis J, Carlson G, Hutton M, Ashe KH. Age-dependent neurofibrillary tangle formation, neuron loss, and memory impairment in a mouse model of human tauopathy (P301L). J Neurosci 2005;25(46):10637–10647. [PubMed: 16291936]

Rocher AB, Crimins JL, Amatrudo JM, Kinson MS, Todd-Brown MA, Lewis J, Luebke JI. Structural and functional changes in tau mutant mice neurons are not linked to the presence of NFTs. Exp Neurol. 2010 (in press).

Rodriguez A, Ehlenberger D, Kelliher K, Einstein M, Henderson SC, Morrison JH, Hof PR, Wearne SL. Automated reconstruction of three-dimensional neuronal morphology from laser scanning microscopy images. Methods 2003;30(1):94–105. [PubMed: 12695107]

Rodriguez A, Ehlenberger DB, Hof PR, Wearne SL. Rayburst sampling, an algorithm for automated three-dimensional shape analysis from laser scanning microscopy images. Nat Protoc 2006;1(4):2152–2161. [PubMed: 17487207]

Rodriguez A, Ehlenberger DB, Dickstein DL, Hof PR, Wearne SL. Automated three-dimensional detection and shape classification of dendritic spines from fluorescence microscopy images. PLoS One 2008;3(4):e1997. [PubMed: 18431482]

Scheff SW, Price DA. Alzheimer's disease-related alterations in synaptic density: neocortex and hippocampus. J Alzheimers Dis 2006;9(Suppl 3):101–115. [PubMed: 16914849]

Scheff SW, Price DA, Schmitt FA, DeKosky ST, Mufson EJ. Synaptic alterations in CA1 in mild Alzheimer disease and mild cognitive impairment. Neurology 2007;68(18):1501–1508. [PubMed: 17470753]

Segal M. Dendritic spines and long-term plasticity. Nat Rev Neurosci 2005;6(4):277–284. [PubMed: 15803159]

Shahani N, Brandt R. Functions and malfunctions of the tau proteins. Cell Mol Life Sci 2002;59(10): 1668–1680. [PubMed: 12475178]

Sholl DA. Dendritic organization in the neurons of the visual and motor cortices of the cat. J Anat 1953;87(4):387–406. [PubMed: 13117757]

Soloway AS, Pucak ML, Melchitzky DS, Lewis DA. Dendritic morphology of callosal and ipsilateral projection neurons in monkey prefrontal cortex. Neuroscience 2002;109(3):461–471. [PubMed: 11823059]

Sommer B, Monyer H, Wisden W, Verdoorn TA, Burnashev N, Sprengel R, Sakmann B, Seeburg PH. Glutamate-gated ion channels in the brain. Genetic mechanism for generating molecular and functional diversity. Arzneimittelforschung 1992;42(2A):209–210. [PubMed: 1375026]

Spillantini MG, Van Swieten JC, Goedert M. Tau gene mutations in frontotemporal dementia and parkinsonism linked to chromosome 17 (FTDP-17). Neurogenetics 2000;2(4):193–205. [PubMed: 10983715]

Spires TL, Orne JD, SantaCruz K, Pitstick R, Carlson GA, Ashe KH, Hyman BT. Region-specific dissociation of neuronal loss and neurofibrillary pathology in a mouse model of tauopathy. Am J Pathol 2006;168(5):1598–1607. [PubMed: 16651626]

Tackenberg C, Brandt R. Divergent pathways mediate spine alterations and cell death induced by amyloid-beta, wild-type tau, and R406W tau. J Neurosci 2009;29(46):14439–14450. [PubMed: 19923278]

Tackenberg C, Ghori A, Brandt R. Thin, stubby or mushroom: spine pathology in Alzheimer's disease. Curr Alzheimer Res 2009;6(3):261–268. [PubMed: 19519307]

Terry RD, Masliah E, Salmon DP, Butters N, DeTeresa R, Hill R, Hansen LA, Katzman R. Physical basis of cognitive alterations in Alzheimer's disease: synapse loss is the major correlate of cognitive impairment. Ann Neurol 1991;30(4):572–580. [PubMed: 1789684]

Thies E, Mandelkow EM. Missorting of tau in neurons causes degeneration of synapses that can be rescued by the kinase MARK2/Par-1. J Neurosci 2007;27(11):2896–2907. [PubMed: 17360912]

Tucker KL, Meyer M, Barde YA. Neurotrophins are required for nerve growth during development. Nat Neurosci 2001;4(1):29–37. [PubMed: 11135642]

Wearne SL, Rodriguez A, Ehlenberger DB, Rocher AB, Henderson SC, Hof PR. New techniques for imaging, digitization and analysis of three-dimensional neural morphology on multiple scales. Neuroscience 2005;136(3):661–680. [PubMed: 16344143]

Yoshiyama Y, Uryu K, Higuchi M, Longhi L, Hoover R, Fujimoto S, McIntosh T, Lee VM, Trojanowski JQ. Enhanced neurofibrillary tangle formation, cerebral atrophy, and cognitive deficits induced by repetitive mild brain injury in a transgenic tauopathy mouse model. J Neurotrauma 2005;22(10):1134–1141. [PubMed: 16238489]

Yuste R, Bonhoeffer T. Morphological changes in dendritic spines associated with long-term synaptic plasticity. Annu Rev Neurosci 2001;24:1071–1089. [PubMed: 11520928]

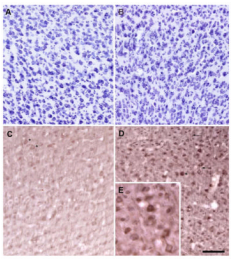

Fig. 1.

Abnormal accumulation of phosphorylated tau in cell bodies and dendrites of PFC neurons of htau mice occurs with age with no apparent changes to neuronal density. Cresyl violet staining of layer III PFC in 3-month-old (**a**) and 12-month-old (**b**) htau mice show no apparent differences in neuronal density. Immunohistochemistry using antibody AT8 reveals the presence of hyperphosphorylated tau in the somata (*asterisks*) and dendrites (*arrow*) of htau mice at 3 months (**c**) and 12 months (**d**) of age. **e** Higher magnification of AT8-immunoreactive neurons from **d**. AT8 immunoreactivity was stronger in the older htau mice. *Scale bar* 80 μm

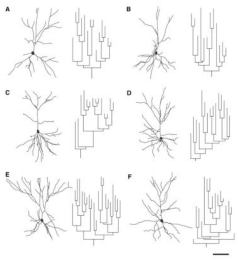

Fig. 2.

Representative examples of 3D reconstructions from layer III PFC neurons from 3-, 6-, and 12-month-old htau mice. Reconstructed cells and corresponding apical dendrite dendrograms from 3-month-old htau (**a**) and wt (**b**), 6-month-old htau (**c**) and wt (**d**), and 12-month-old htau (**e**) and wt (**f**) old mice were obtained using NeuroExplorer (MBF Bioscience). Neurons were rotated about their principal axis to depict their apical and basal dendritic orientation. *Scale bar* 50 μm

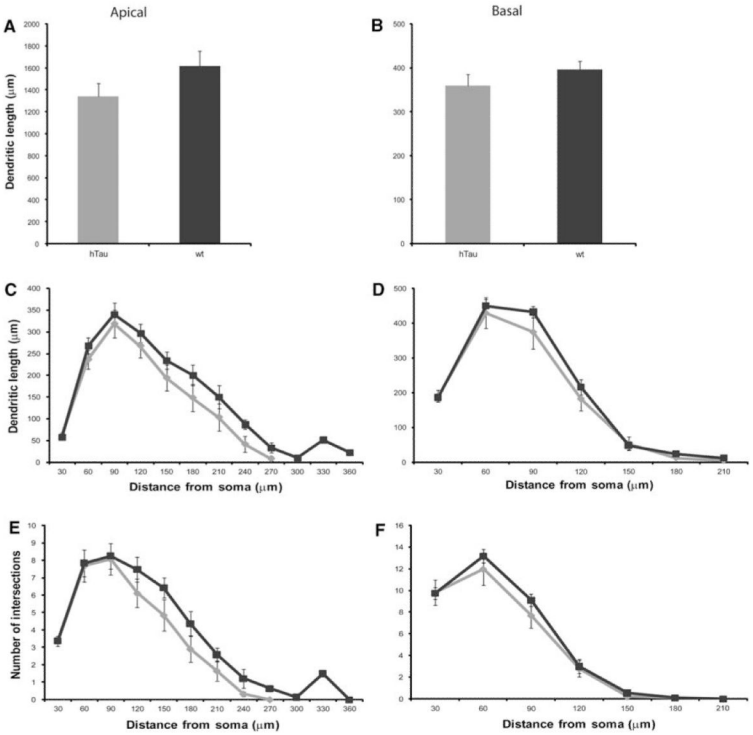

Fig. 3.

Dendritic morphologic alterations as a function of genotype in layer III PFC pyramidal neurons of 3-month-old htau and wt mice. Dendritic length and Sholl analyses in apical (**a, c, e**) and basal (**b, d, f**) dendrites of layer III PFC pyramidal cells of 3-month-old htau mice (*light gray*) and wt mice (*black*) were traced in 3D using Neurolucida and quantified using NeuroExplorer (MBF Bioscience). *Asterisks* indicate statistically significant differences; *$p < 0.05$. Values represent mean ± SEM

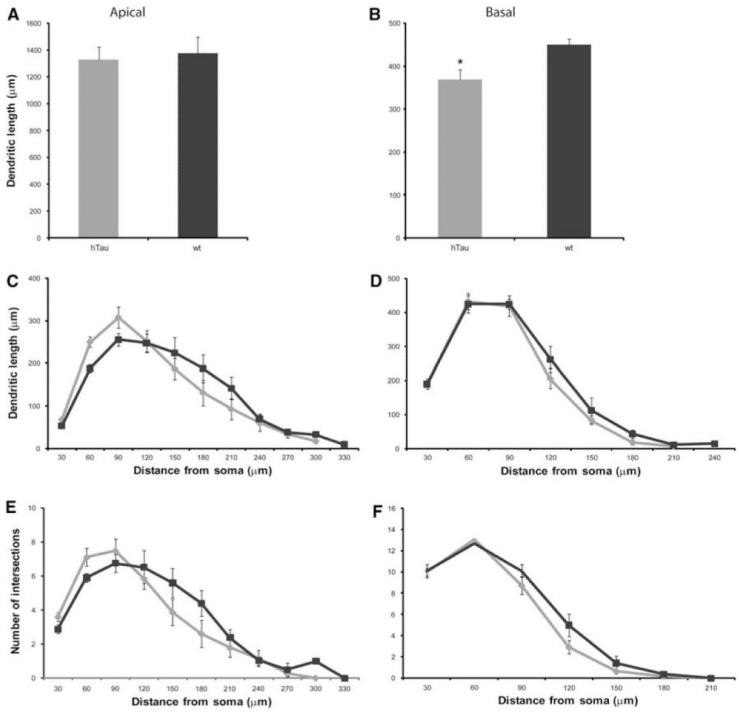

Fig. 4.

Dendritic morphologic alterations as a function of genotype in layer III PFC pyramidal neurons of 6-month-old htau and wt mice. Dendritic length and Sholl analyses in apical (**a, c, e**) and basal (**b, d, f**) dendrites of layer III PFC pyramidal cells of 6-month-old htau mice (*light gray*) and wt mice (*black*) were traced in 3D using Neurolucida (MBF Bioscience) and quantified using NeuroExplorer (MBF Bioscience). *Asterisks* indicate statistically significant differences; *$p < 0.05$. Values represent mean ± SEM

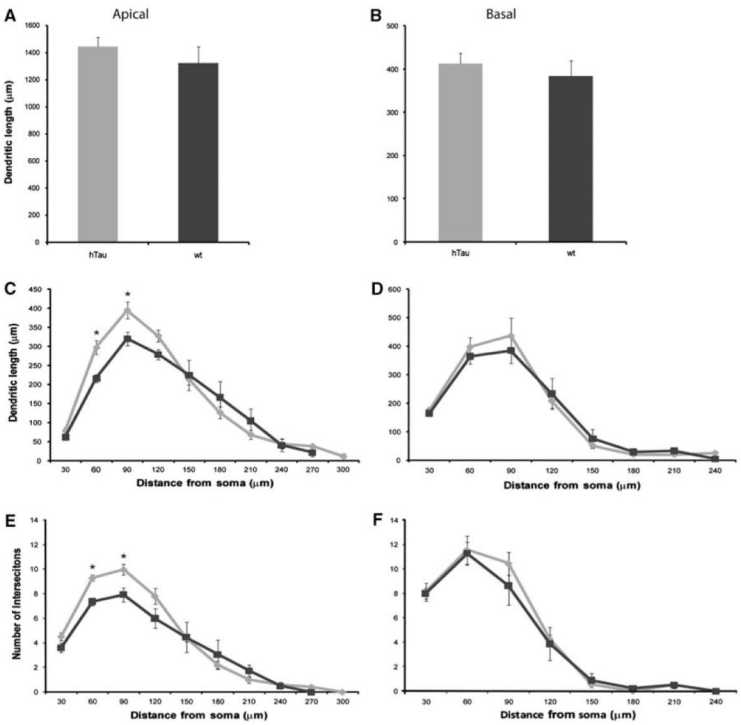

Fig. 5.

Dendritic morphological alterations as a function of genotype in layer III PFC pyramidal neurons of 12-month-old htau and wt mice. Dendritic length and Sholl analyses in apical (**a, c, e**) and basal (**b, d, f**) dendrites of layer III PFC pyramidal cells of 12-month-old htau mice (*light gray*) and wt mice (*black*) were traced in 3D using Neurolucida (MBF Bioscience) and quantified using NeuroExplorer (MBF Bioscience). *Asterisks* indicate statistically significant differences; *$p < 0.05$. Values represent mean ± SEM

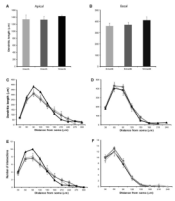

Fig. 6.

Dendritic morphological alterations as a function of age in layer III PFC pyramidal neurons in the htau mouse. Dendritic length and Sholl analyses in apical (**a, c, e**) and basal (**b, d, f**) dendrites of layer III PFC pyramidal cells of htau mice at 3 (*light gray*), 6 (*dark gray*), and 12 months (*black*) of age were traced in 3D using Neurolucida (MBF Bioscience) and quantified using NeuroExplorer (MBF Bioscience). *Asterisks* indicate statistically significant differences; $*p < 0.05$. Values represent mean ± SEM

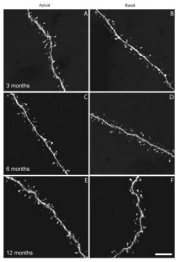

Fig. 7.

Three-dimensional digital reconstructions of apical and basal dendritic segments from 3-, 6-, and 12-month-old htau mice. **a, b** Apical and basal dendrites at 3 months, **c, d** apical and basal dendrites at 6 months, and **e, f** apical and basal dendrites at 12 months. Note the clear resolution of spine morphologies. *Scale bar* 5 μm

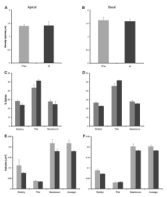

Fig. 8.

Spine alterations as a function of genotype in layer III PFC pyramidal neurons in 3-month-old htau versus wt mice. **a, b** Spine density, **c, d** spine type, and **e, f** spine volume in 6-month-old htau mice (*gray*), and 12-month-old wt mice (*black*) from layer III PFC pyramidal neurons analyzed using NeuronStudio. *Asterisks* indicate statistically significant differences; $*p < 0.05$. Values represent mean ± SEM

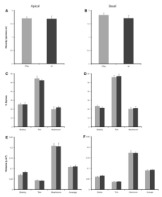

Fig. 9.

Spine alterations as a function of genotype in layer III PFC pyramidal neurons in 6-month-old htau versus wt mice. **a, b** Spine density, **c, d** spine type, and **e, f** spine volume in 6-month-old htau mice (*gray*) 12-month-old wt mice (*black*) from layer III PFC pyramidal neurons analyzed using NeuronStudio. *Asterisks* indicate statistically significant differences; $*p < 0.05$. Values represent mean ± SEM

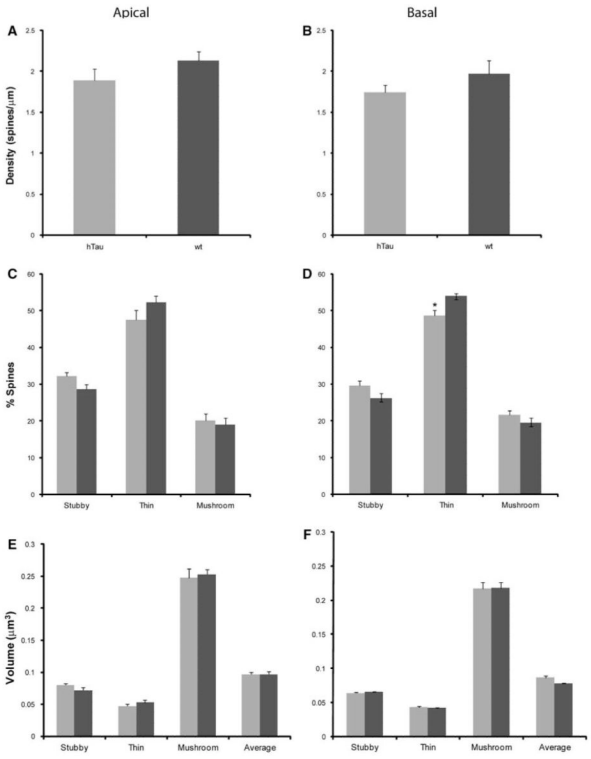

Fig. 10.

Spine alterations as a function of genotype in layer III PFC pyramidal neurons in 12-month-old htau versus wt mice. **a, b** Spine density, **c, d** spine type, and **e, f** spine volume in 12-month-old htau mice (*gray*) 12-month-old wt mice (*black*) from layer III PFC pyramidal neurons analyzed using NeuronStudio. *Asterisks* indicate statistically significant differences; $*p < 0.05$. Values represent mean ± SEM

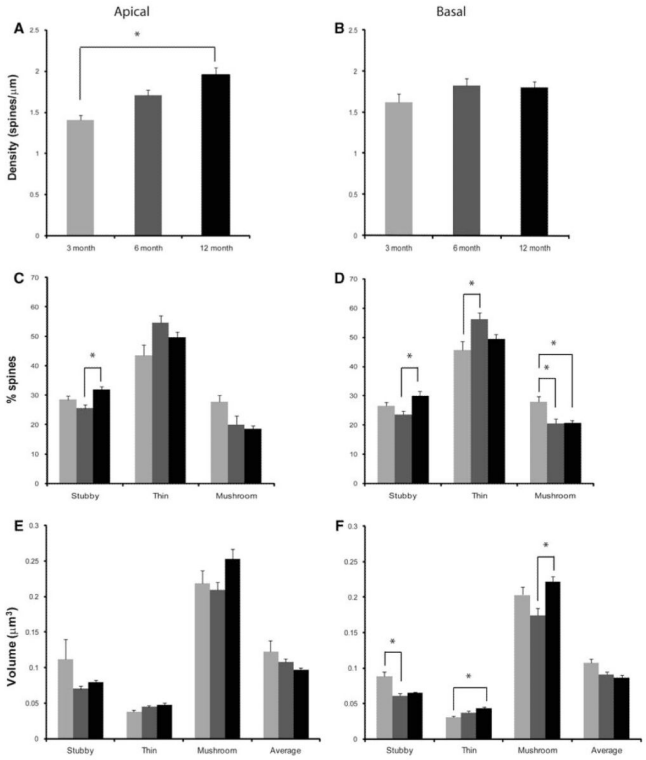

Fig. 11.

Spine alterations as a function of age in layer III PFC pyramidal neurons of the htau mouse. **a, b** Spine density, **c, d** spine type, and **e, f** spine volume in 3- (*light gray*), 6- (*dark gray*), and 12-month-old mice (*black*) from layer III PFC pyramidal neurons analyzed using NeuronStudio. *Asterisks* indicate statistically significant differences; $*p < 0.05$. Values represent mean ± SEM

Table 1

Sample size for all neuron morphologic and spine analyses at various time points

Analysis	Age (months)	Sample size (no. of mice)		Sample size (average no. of neurons or dendrites)	
		htau	wt	htau	wt
Neuron morphology	3	5	5	5	5
Spine analysis	3	3	3	50	43
Neuron morphology	6	6	6	5	5
Spine analysis	6	5	4	68.5	75
Neuron morphology	12	7[a]	5[a]	5	5
Spine analysis	12	5	3	148	63.5

For morphologic data, sample size refers to number of neurons per animal, and for spine data sample size refers to total number of dendrites. For each animal a minimum of three dendrites per neuron was analyzed

[a]For this time point there was one fewer wt animal for apical Sholl and apical intersection analysis, and one fewer htau animal for the basal dendritic analysis

Table 2

Dendrite and spine morphometry from layer III pyramidal neurons from htau and wt mice at 3, 6, and 12 months of age

Genotype	Morphology (μm)		Spine				
			Density (spines/μm)		Type (%)		
	Apical	Basal	Apical	Basal	Apical		
					S	T	M
3 months							
htau	1,338.6 ± 123.8	359.0 ± 26.4	1.40 ± 0.06	1.62 ± 0.11	28.42 ± 1.34	43.5 ± 3.59	27.81 ± 2.11
wt	1,635.4 ± 134.7	395.9 ± 19.8	1.42 ± 0.17	1.58 ± 0.09	23.96 ± 1.53	51.52 ± 1.47	24.81 ± 3.16
6 months							
htau	1,330.0 ± 94.4	**369.7 ± 22.6** *	1.70 ± 0.06	1.83 ± 0.08	25.44 ± 1.27	54.58 ± 2.52	20.0 ± 2.97
wt	1,374.8 ± 125.7	**451.2 ± 12.9** *	1.69 ± 0.11	1.71 ± 0.1	25.46 ± 1.98	52.46 ± 1.13	21.96 ± 1.47
12 months							
htau	1,429.5 ± 31.7	411.1 ± 28.8	1.96 ± 0.09	1.80 ± 0.07	31.92 ± 1.04	49.65 ± 1.86	18.45 ± 1.14
wt	1,382.9 ± 262.6	341.4 ± 39.9	2.13 ± 0.11	1.97 ± 0.16	28.69 ± 1.24	52.26 ± 1.74	19.02 ± 1.84

Genotype	Spine								
	Type (%)			Volume (μm^3)					
	Basal			Apical			Basal		
	S	T	M	S	T	M	S	T	M
3 months									
htau	26.51 ± 1.25	45.56 ± 2.97	27.88 ± 1.77	0.11 ± 0.03	0.04 ± 0.002	0.22 ± 0.02	0.09 ± 0.01	0.03 ± 0.002	0.20 ± 0.01
wt	22.86 ± 0.53	51.86 ± 0.49	25.61 ± 0.32	0.07 ± 0.003	0.03 ± 0.001	0.18 ± 0.004	0.07 ± 0.001	0.03 ± 0.002	0.18 ± 0.001
6 months									
htau	23.45 ± 1.27	56.12 ± 2.21	20.44 ± 1.62	0.07 ± 0.004	0.04 ± 0.002	0.21 ± 0.01	0.06 ± 0.004	0.04 ± 0.001	0.17 ± 0.01
wt	21.53 ± 1.27	57.29 ± 2.33	21.26 ± 1.97	0.08 ± 0.005	0.04 ± 0.003	0.21 ± 0.106	0.07 ± 0.002	0.04 ± 0.001	0.17 ± 0.005
12 months									
htau	29.96 ± 1.52	**49.4 ± 1.57** *	20.64 ± 0.85	0.08 ± 0.002	0.05 ± 0.003	0.25 ± 0.01	0.06 ± 0.001	0.04 ± 0.001	0.22 ± 0.01
wt	26.30 ± 1.25	**54.11 ± 0.58** *	19.51 ± 1.38	0.07 ± 0.005	0.05 ± 0.003	0.25 ± 0.01	0.06 ± 0.001	0.04 ± 0.001	0.22 ± 0.01

S stubby spine, *T* thin spine, *M* mushroom spine

* $p<0.05$

Table 3

Dendrite and spine morphometry from layer III pyramidal neurons from the PFC of htau mice during disease progression

Age (months)	Morphology (μm)		Spine				
			Density (spines/μm)		Type (%)		
	Apical	Basal	Apical	Basal	Apical		
					S	T	M
3	1,338.6 ± 123.8	359.0 ± 26.4	**1.40 ± 0.06**	1.62 ± 0.11	28.42 ± 1.34	**43.5 ± 3.59** *	27.81 ± 2.11
6	1,330.0 ± 94.4	369.7 ± 22.6	1.70 ± 0.06	1.83 ± 0.08	**25.44 ± 1.27** **	**54.58 ± 2.52** *	20.0 ± 2.97
12	1,429.5 ± 31.7	411.1 ± 28.8	**1.96 ± 0.09** **	1.80 ± 0.07	**31.92 ± 1.04** **	49.65 ± 1.86	18.45 ± 1.14

Age (months)	Spine								
	Type (%)			Volume (μm^3)					
	Basal			Apical			Basal		
	S	T	M	S	T	M	S	T	M
3	26.51 ± 1.25	**45.56 ± 2.97** *	**27.88 ± 1.77** *	0.111 ± 0.03	0.038 ± 0.002	0.218 ± 0.02	**0.088 ± 0.01** **	**0.031 ± 0.002** *	0.203 ± 0.01
6	**23.45 ± 1.27** **	**56.12 ± 2.21** *	**20.44 ± 1.62** *	0.069 ± 0.004	0.044 ± 0.002	0.209 ± 0.01	**0.061 ± 0.004** **	0.037 ± 0.001	**0.174 ± 0.01** **
12	**29.96 ± 1.52** **	49.4 ± 1.57	20.64 ± 0.85	0.08 ± 0.002	0.047 ± 0.003	0.252 ± 0.01	0.065 ± 0.001	**0.043 ± 0.001** *	**0.222 ± 0.01** **

S stubby spine, *T* thin spine, *M* mushroom spine

* $p<0.05$,

** $p<0.01$